UNIVERSITYᴼF BIRMINGHAM

University of Birmingham
Research at Birmingham

Processing conditions and mechanisms for the plasma defect-engineering of bulk oxygen-deficient zirconia

Shi, Fangzhou; Dashtbozorg, Behnam; Li, Xiaoying; Dong, Hanshan

[Link to publication on Research at Birmingham portal](#)

Processing conditions and mechanisms for the plasma defect-engineering of bulk oxygen-deficient zirconia

Fangzhou Shi, Behnam Dashtbozorg [*], Xiaoying Li, Hanshan Dong

School of Metallurgy & Materials, University of Birmingham, Birmingham, B15 2TT, UK

ABSTRACT

In recent years, the utilisation of oxygen-deficient zirconia ($ZrO_{2-\alpha}$), commonly referred to as black zirconia, has garnered considerable attention due to its potential applications for solid oxide fuel cells (SOFCs), gas sensors, biomedical implant materials, and photocatalysis. However, current methods employed to manufacture $ZrO_{2-\alpha}$ exhibit noticeable limitations regarding their scalability, environmental sustainability, and cost-effectiveness. Our recent work has successfully demonstrated the feasibility for bulk conversion of conventional white zirconia into oxygen-deficient black zirconia through direct current (DC) plasma treatment (i.e. plasma blackening). This study elucidates the conditions for plasma blackening and provides a unique mechanism for the bulk transformation of zirconia. A systematic investigation of different plasma technologies (DC, active-screen plasma), treatment configurations (contact conditions, cathode material, and cathode potential), and treatment parameters (voltage, temperature, duration) uncover the crucial variables that influence the feasibility and rate of the reduction process. The reduction of zirconia is shown to initiate from localised contacting points at the cathode-facing surface and grow, with a hemispherical shape, towards the anode-facing surface. A series of development stages are proposed for the process, namely: bulk oxygen vacancy conductance, surface activation, oxygen vacancy generation and a moving cathode front. The findings of this study provide insights into the underlying mechanisms involved in the bulk-reduction of zirconia and help to pave the way towards future scalable and cost-effective generation of oxygen-deficient zirconia.

1. Introduction

The reported photocatalytic behaviour of black titanium oxide (TiO_{2-x}) has led to a surge of interest in equivalent black zirconia, known as oxygen-deficient black zirconia ($ZrO_{2-\alpha}$), as a potential alternative next-generation photocatalytic material [1]. The desirable photocatalytic properties of these defect-engineered metal oxide materials have been attributed to an abundance of oxygen vacancies, which generate new mid-gap states around the Fermi level and are accompanied by the remarkable change in optical properties (e.g., change of colour) [2,3]. This approach widens the application range and potential value of black oxygen-deficient ($ZrO_{2-\alpha}$) as an energy harvesting material, for the generation of hydrogen, for the decomposition of pollutants, and for medical applications (e.g., tumour therapy) [4–6].

The phenomenon of colour change is particularly prevalent in specific metal oxides, such as zirconia and titania, renowned for their remarkable capacity to exhibit diverse colours in the presence of cationic dopants [7–12]. Consequently, early research has focused on controlling and fine-tuning the colours of these materials by manipulating the types and concentrations of dopants using various methods, including high-temperature sintering, sol-gel processes, and coprecipitation [13–15].

Subsequent investigations have revealed that the augmentation of optical absorption intensity and photocatalytic activity of zirconia is intimately linked to the presence of surface oxygen vacancies [12, 16–21]. Consequently, this has directed researchers to focus on the effective reduction of zirconia. Although zirconium has a relatively strong affinity for oxygen, a diverse range of elements (e.g., calcium, iron, yttrium) exist that can extract oxygen from zirconia, while simultaneously reducing zirconium ions (Zr^{4+} to Zr^{3+}) [3,22]. Different approaches have been explored, including chemical reduction using methods such as molten lithium reduction [23,24], magnesiothermic reduction in the presence of 5% H_2/Ar [1], reduction of zirconium (IV)-*n*-propoxide (ZrP) solution through sol-gel synthesis [25,26] and

high-pressure torsion [6]. However, these methods for generating blackened zirconia are characterised by several inherent limitations, including long production cycles, use of hazardous chemical reagents, low efficiency, high energy consumption, and environmental concerns (e.g., disposal of chemical reagents). Furthermore, the majority of the reduced black zirconia manufactured under these approaches are in powder form and require sintering into bulk components for applications demanding structural integrity, specific geometries and resistance to mechanical stresses. Re-oxidation is difficult, if not impossible, to avoid when sintering oxygen-deficient zirconia, and therefore predominantly limits the use of the material to its powder form [3,23,27].

To address these technological and environmental challenges, the authors of this study have recently successfully reported a novel approach employing low-pressure plasma to produce bulk oxygen-deficient zirconia with excellent broad spectrum light absorption capability [28]. However, as only a single DC plasma treatment condition (500 °C at 300 Pa for 5 hours in 100% H_2) has been reported thus far, the underlying mechanisms involved, and the influence of different treatment conditions are not yet established.

Consequently, this study aims to investigate the underlying mechanisms involved through systematic evaluation of the role of different treatment parameters on the generation of oxygen-deficient zirconia. These parameters include different types of plasma technologies (DC plasma and active-screen plasma), DC plasma treatment configurations (contact conditions and cathode material), and plasma treatment conditions (voltage, temperature and duration). It is expected that the outcomes of this investigation will both advance scientific understanding of the mechanism involved in the plasma blackening of zirconia and contribute to the future development and optimisation of this novel, cost-effective, and environmentally friendly plasma defect-engineering manufacturing route.

2. Methods

2.1. Sample preparation

The samples used in this study were cut from 3 mol-% yttria-stabilised tetragonal zirconia rods into cylindrical coupons with a thickness of 3 mm and a diameter of 10 mm using a Struers Accutom 50 machine and a cubic boron nitride cutting wheel. The cylindrical coupon samples were ground to #1200 grit size SiC paper before polishing using diamond suspensions with particle sizes of 6, 3, and 1 μm.

2.2. Plasma treatment configurations

The plasma treatments were performed using a Klöckner Ionon 40 kVA plasma furnace. Specific overviews of the difference treatment setups, treatment parameters and treatment configurations utilised in this study are described in the following sections.

2.2.1. Plasma treatment setups

To investigate the effect of direct cathode power of the worktable (where the sample is placed), both DC (direct current) and active-screen (AS) plasma setups were employed. The samples were placed directly onto the worktable connected to the cathode in the DC plasma treatment setup (Fig. 1a), while the samples were electrically isolated from the cathode (i.e., at a floating potential) in the AS plasma treatments. An AISI 316 austenitic stainless steel mesh cage and lid, known as the active screen, were connected to the cathode and placed around the isolated sample in the AS plasma treatment (Fig. 1b). A distance of 20 mm was kept between the sample surface and the active screen lid. Both DC and AS plasma treatments were carried out at 500 °C for 5 hours in H_2 gas at 3 mbar (300Pa).

2.2.2. Plasma treatment parameters

The effect of DC plasma treatment parameters on the blackening of zirconia were systematically studied using a range of the treatment temperatures (ranging from 100 to 500 °C) and treatment durations (30 and 300 min).

Investigations related to the effect of treatment voltages were carried out between 370 and 450 V. Given that the furnace voltage and the chamber temperature are inherently linked (with larger temperatures requiring larger DC voltages), it was necessary to incorporate auxiliary heating sources to isolate the two key variables. Consequently, a secondary DC power supply (TRUMPF TruPlasma DC 3005) was employed to enable the initial heating up ramp to be conducted without any power to the sample and to compensate for the varying thermal power provided by the different applied voltages. In this approach, the furnace power was used as an auxiliary heating source (indirectly heating samples and maintaining the chamber temperature), while the secondary DC power source acted as the main cathode power source (Fig. 2).

2.2.3. Plasma treatment configurations

To verify whether the cationic doping from the metallic ions in the steel worktable was dictating the treatment of zirconia, separate plasma treatments were performed (at 500 °C for 5h) using worktables composed of zirconium (Zr 702) and AISI 316 stainless steel (as shown in Fig. 3).

Similarly, to study the influence of contact conditions on the initiation of the black spots on the cathode-facing surface, two different AISI 316 stainless steel base samples were designed with and without blind holes (as depicted in Fig. 4). The diameter of each stainless-steel block
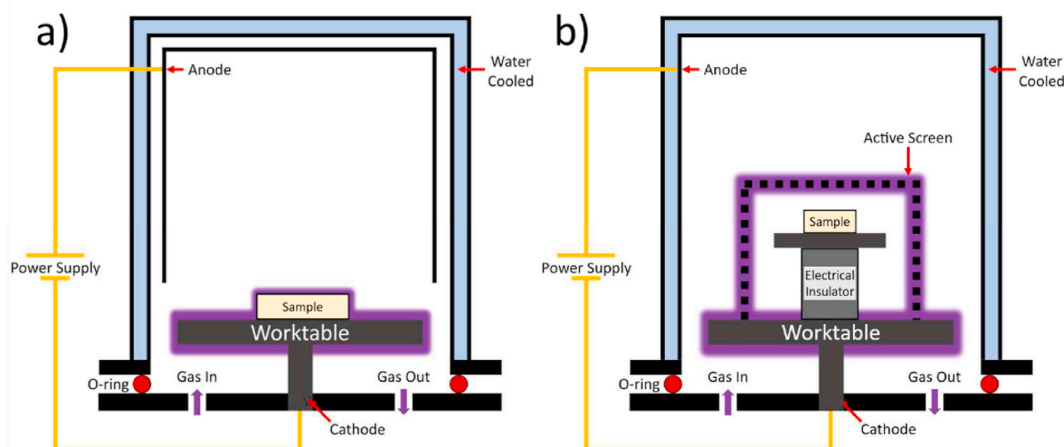

Fig. 1. Schematic diagram of (a) DC and (b) AS plasma treatment setups (modified from Ref. [29]).
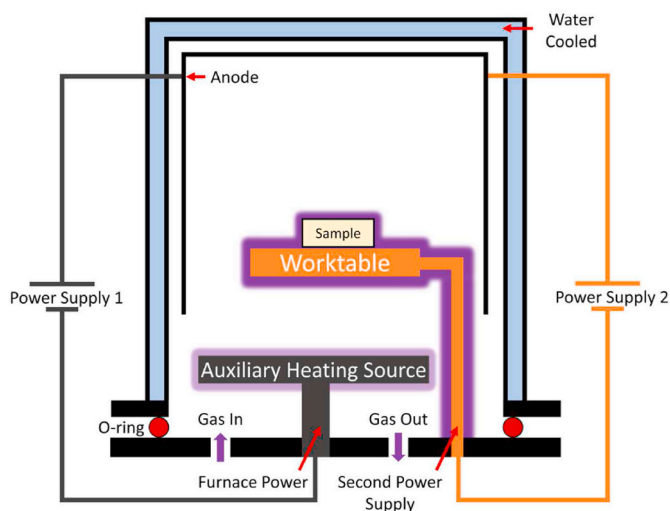
Fig. 2. Schematic diagram of the plasma treatment setup with two DC power sources.

was chosen to match the size of the sample (to limit the formation of hollow cathodes at the bottom edges of the samples). The temperature was set at 200 °C, and the durations chosen were 30 and 300 min.

Furthermore, to investigate whether the black regions always grow from the bottom to the top of the material, or whether they grow from the cathode-facing surface towards the opposite-facing surface (denoted as anode-facing surface), a treatment configuration was employed where the contact point of the zirconia sample with the cathode was changed to be at the top surface (as shown in Fig. 5).

2.3. Raman mapping

Raman scanning was conducted using a Renishaw inVia Raman microscope fitted with a 532 nm excitation laser source and groove density of 1800 l/mm. Raman reflectivity was employed to characterise the bulk modification of zirconia. The data was processed using Casa XPS for deconvolution of the spectra (into the 3 E_g and 1 A_{1g} modes of the

tetragonal phase). The data was finally analysed by accumulating the area contributions of all 4 tetragonal phase peaks into intensity maps across the depth of the samples.

3. Experimental results

3.1. Effect of the different plasma setups (DC and AS)

As described in §2.2, both DC plasma (DCP) and AS plasma (ASP) treatment configurations were employed to study the impact of direct cathodic potential on the plasma blackening of zirconia.

Fig. 6 reveals that the white zirconia could only be completely transformed to black under DCP-treatment whilst the ASP treated samples have no appreciable transformation in colour. Therefore, this confirms the need for direct power to the sample for the successful plasma blackening of zirconia (which will be further discussed in §4).

3.2. Effect of plasma treatment parameters

Given that only DCP treatments were able to modify the zirconia (Fig. 6), all subsequent investigations were exclusively performed under DCP treatment conditions. The key parameters considered in these experiments were the treatment temperatures (100, 200, 300, and 500 °C),
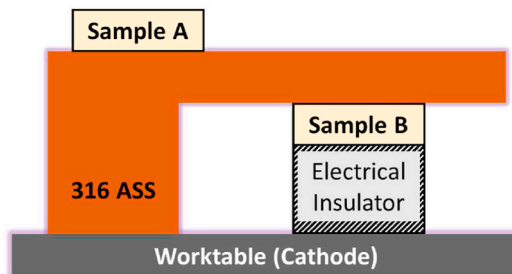
Fig. 5. Schematic diagram of the plasma treatment configuration investigating the direction of growth. Sample A was placed with the bottom surface in contact with the cathode (AISI 316 austenitic stainless steel). Sample B was placed with the top surface in contact with the cathode.
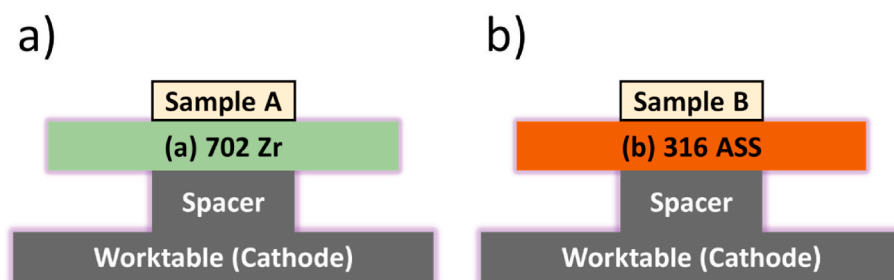
Fig. 3. Schematic diagram of DCP treatment with different sample worktable materials: (a) Zr702 and (b) AISI 316 stainless steel.
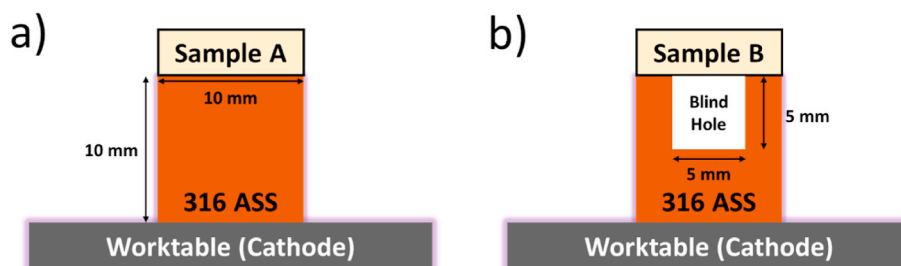
Fig. 4. Schematic design and configuration of the DC plasma treatment with (a) normal and (b) blind hole contact conditions.
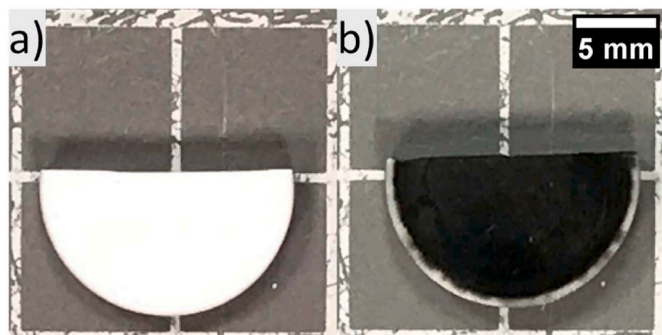
Fig. 6. Surface images of (a) ASP-treated and (b) DCP-treated zirconia.

durations (30 and 300 min) and applied cathodic potential (370–450 V).

3.2.1. Temperature & duration

Fig. 7 reveals a positive correlation between the degree of plasma blackening for both treatment temperature and duration. As evidenced in Fig. 7a1 and a2, there is no appreciable blackening when treatment was performed at 100 °C, even when the sample was treated for 5 hours. Colour transformation (blackening) was observed to initiate when the temperature was increased to 200 °C, appearing to grow from the bottom cathode-facing surface of the samples. Moreover, a significant increase in the depth of the black region was found when the treatment duration was extended from 30 min to 5 hours (Fig. 7b1 and b2).

A significant increase in the degree of blackening was observed when the treatment temperature was increase to 300 °C. Fig. 7c1 and c2 clearly illustrate that the samples become almost entirely black, even when treated for only 30 min. The initially discrete black spots on the surface of the sample are found to merge, forming a continuous black surface. Internally, striations of lighter and darker regions are found to develop across the sample, forming columns that traverse from the bottom to the top of the sample. Additionally, the colour of the material close to the bottom (cathode-facing) surface is found to be darker than the top (anode-facing) surface, with a gradual change of colour, going

from black to reddish-brown, within each column. At 500 °C, these colour variations are not as visible, with both surfaces presenting with a deep and uniform black colour (Fig. 7d1 and d2). The only notable difference between the samples treated at 500 °C for 30 min and 5 hours is the transformation (blackening) of minor regions near the edges of the top surface.

Overall, these observations signify that the treatment temperature has a substantial effect on the feasibility and degree of plasma blackening of zirconia, while the treatment duration appears to only have an accumulative effect on the degree of plasma-induced blackening.

3.2.2. Effect of cathode voltage

As no appreciable glow-discharge was observed within the plasma furnace at voltages below 370 V, the influence of cathodic potential was only examined at voltages greater than 370 V. Simultaneously, it was not possible to maintain a temperature of 200 °C with the application of potentials above 450 V (temperature increased above 200 °C even with just a single power source). Therefore, investigations on the influence of cathodic potential on the plasma blackening of zirconia were limited to voltages between 370 and 450 V.

As revealed within Fig. 8, when all other parameters are controlled, the influence of increasing voltage is found to directly correlate with the number of circular black spots formed on the cathode-facing (bottom) surface of the zirconia sample. Given the varying sizes of the spots between and within each sample, only the largest (i.e., fastest growing) spots were used for comparisons between different voltage settings. No significant difference could be measured in the diameters of the largest black spot formed across the different voltage treatments, with an overall average diameter of 1.97 ± 0.06 mm. As the frequency of the formed spots increases with applied voltage, this implies that cathodic voltage plays an important role for initiating the transformation but does not appear to significantly impact the growth mechanism.

3.3. The effect of plasma treatment settings

As the materials involved and configuration of the plasma furnace can also impact the outcome of the treatment, the following chapter
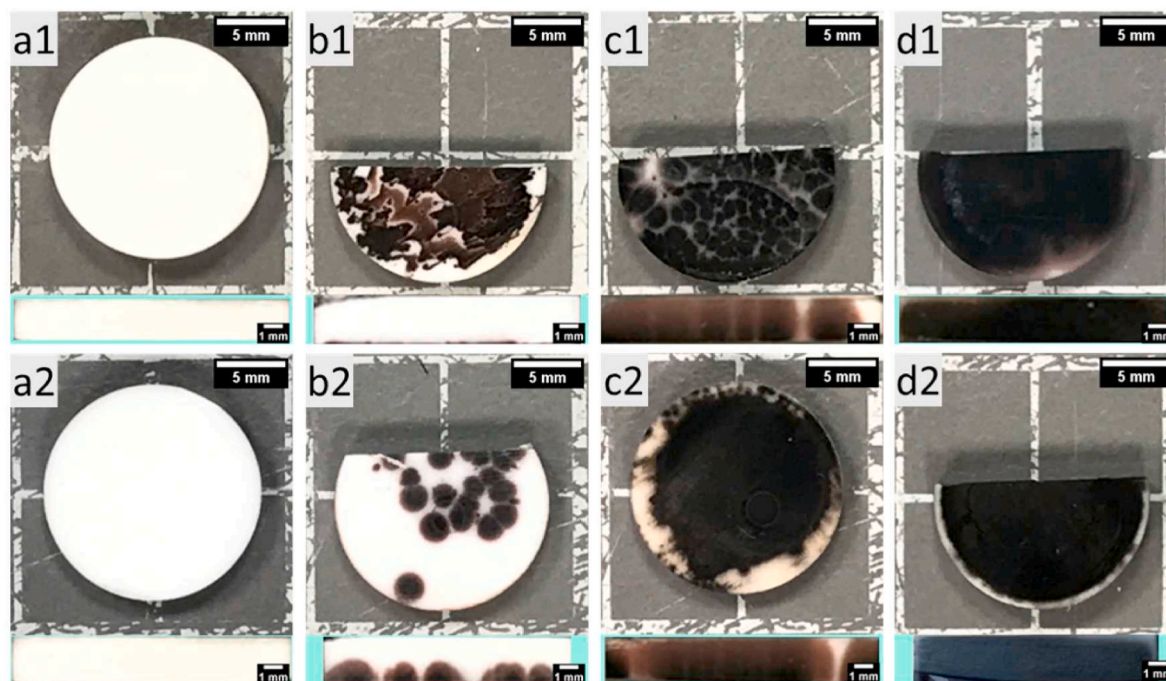

Fig. 7. Optical images of zirconia samples DC plasma treated under different temperatures of (a) 100 °C, (b) 200 °C, (c) 300 °C, and (d) 500 °C. Treatment durations of (1) 30 min and (2) 5 hours are also shown for each temperature. A cross-section view of each treated sample is also present at the bottom of each image.
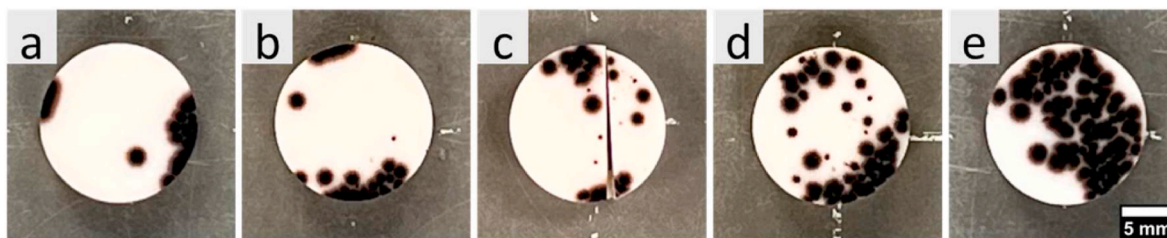
Fig. 8. Optical images of zirconia samples DC plasma treated under different cathode potentials of (a) 370 V, (b) 390 V, (c) 410 V, (d) 430 V, and (e) 450 V.

aims to assess the potential role of cationic doping on the transformation of zirconia, the need for direct contact with the cathode for the initiation and growth of black regions, and the direction of growth of the black regions.

3.3.1. Cathode material

Cationic doping (e.g., with Fe) has previously been reported to be able to reduce zirconia, thereby transforming the material from white to black [15,30–32]. Given that the steel cathode worktable used in this study contains elements which have potential to dope zirconia, it is important to investigate plasma treatments where cationic doping is not possible (or significantly restricted). Since Zr702 is primarily composed of Zr (98.8 wt%), the potential role of cationic doping can be effectively avoided when carrying out plasma treatments using a Zr702 cathode worktable. As illustrated in Fig. 9, both Zr702 and the AISI 316 stainless-steel cathode materials were able to produce black zirconia, which indicates that the principal mechanism for the plasma blackening of zirconia is independent of elemental doping.

3.3.2. Contact conditions

As the plasma blackening was observed to start at 200 °C (for both 30 min and 5 hour treatments) but did not show complete through-depth treatment of the zirconia, it was chosen as the ideal temperature for examining the importance of contact conditions on the initiation of the blackening. As expected, both the normal and blind hole contact conditions showed that the black spots on the cathode-facing surface (Fig. 10) and the blackened regions of the cross-section (Fig. 11) expanded with longer treatment durations.

Examination of the location and growth of the black spots on the cathode-facing surface of the treated samples demonstrated the importance of direct (or close) contact of the cathode with the sample. Where contact was not possible (i.e., in the blind hole regions), no black spots were found to form (Fig. 10b1-b5). Instead, these areas were only found to begin transforming with longer durations (associated with the accumulation effect, as observed in §3.2.1). On the other hand, under normal contact conditions (Fig. 10a1-a5), both the edges and the centres of the cathode-facing surface were found to form the initial black spots.

Interestingly, the transverse cuts of both treated samples clearly reveal incremental growth of the black regions towards the anode-facing surface (Fig. 11). These initial black dots are found to expand at

approximately equal rates in both the horizontal and vertical directions in the 2D cross-section views. Given the eventual expected through-depth treatment of the zirconia (Fig. 6), this implies that the rate of growth of the black spots is equal in all 3 dimensions (i.e., x, y and z), and therefore should form a hemispherical shape.

3.3.3. Plasma blackening growth direction

Studies utilising electrochemical reduction methods to form black oxygen-deficient zirconia have previously shown that the black regions grow from the cathode towards the anode [33–36]. The similarities between electrochemical reduction techniques and our plasma approach (i.e., both involve the use of separated electrodes) suggest that a similar growth mechanism is to be expected. However, given that plasma treatments also involve ion bombardment of the exposed surfaces (i.e., surfaces not in contact with the cathode) and that the treatments are performed at low pressures, it is still necessary to confirm the direction of growth.

To evaluate the initiation and direction of growth of the black regions, treatments were carried out where the contact point between the cathode and the zirconia samples was reversed (Fig. 5). One sample was maintained in an upright configuration (Sample A; bottom surface in contact with the cathode) while the contact point was flipped for the other sample (Sample B; top surface in contact with the cathode). To allow for the identification of the growth direction, the treatments were performed at a relatively low temperature of 200 °C to avoid the complete transformation of the material.

Fig. 12 reveals that the initiation and growth of the black regions develop from the surfaces in contact with the cathode (i.e., cathode-facing surface). Therefore, this suggests that plasma-induced blackening of zirconia follows the same cathode-to-anode growth direction as the electrochemical reduction methods. Moreover, these findings also support the contact condition requirements for the initiation and growth of the black regions (as previously introduced in §3.3.2).

3.4. Accumulation and degree of blackening

As previously reported by the authors of this study [28], plasma treatments have the ability to significantly improve the broad spectrum light absorption capability of zirconia. Therefore, to map the light absorption capability across a plasma treated zirconia sample, tetragonal phase peak contributions in Raman spectra were systematically collected at different positions across sample. Colour maps were then used to visualise the light absorption capability (or degree of blackening) across the material.

The darkest regions in Fig. 13b appear to correspond with the initial spots at the cathode-facing surface of the sample, which is consistent with the results from §3.3.2 and §3.3.3. The light absorption capability of each black region decreases when moving away from this starting central spot (in all directions). Although isolated black regions were previously observed to grow at the same rate in all directions over time (Fig. 11), when they approach other black regions, they appear to not completely follow this trend. This is clearly found within the highlighted right region of Fig. 13, which shows that the growth of two nearby discrete black regions is hindered at the sides facing each other,
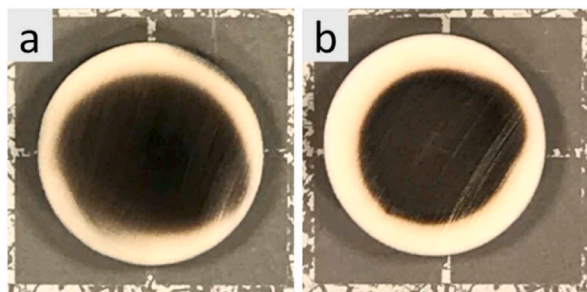

Fig. 9. Optical images after DC plasma treatment at 500 °C for 5 hours using a (a) Zr702 and (b) AISI 316 stainless steel worktable.
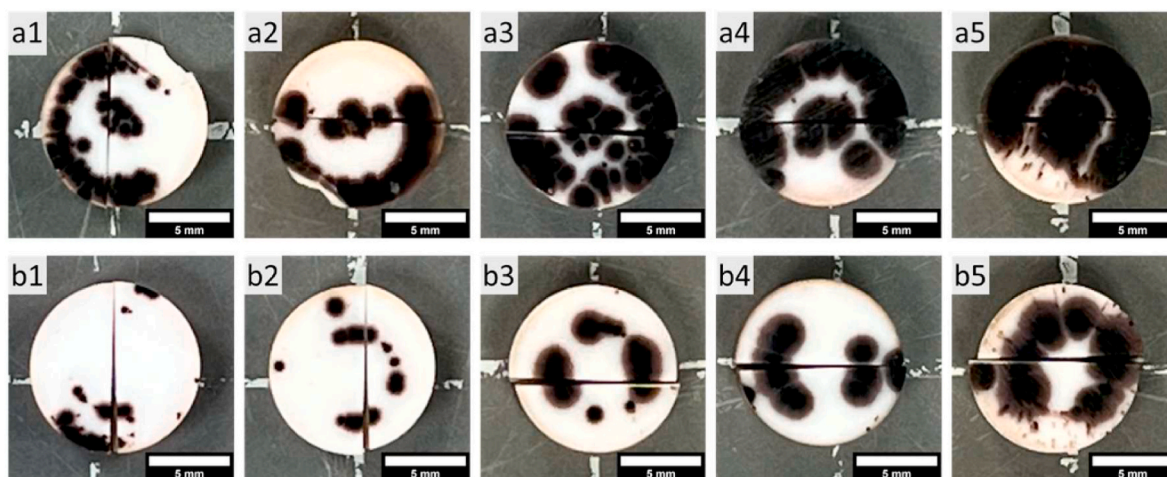
Fig. 10. Plasma treated samples under (a) normal) and (b) blind hole contact conditions at 200 °C for: 1h (1), 2h (2), 3h (3), 4h (4), and 5h (5).
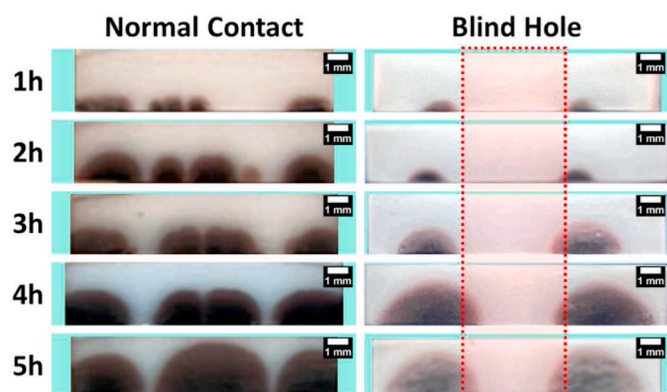

Fig. 11. Cross-section views of plasma treated samples under normal (left) and blind hole (right) contact conditions at 200 °C for increasing durations (going down). Red dashed box highlights the lack of initial transformation wthin the blind hole regions.

therefore suggesting some form of growth inhibition. Interestingly, this is not observed to significantly impact the maximum depth of the black regions, with all black regions appearing to have similar maximum depths.

4. Discussion

To devise the potential transformation mechanism involved during the plasma blackening of zirconia, an evaluation of the influence that different treatment configurations and parameters have on the initiation and growth of black zirconia has been conducted. Given the vast number of parameters, the following discussion has been grouped to overview (1) the role that pre-existing oxygen vacancies have at the start of the plasma treatment, (2) the importance of cathodic contact and electrical discharge on the blackening of zirconia, (3) potential mechanisms for the conductance of oxygen anions within the lattice and the generation of new oxygen vacancies, and (4) the formation of a moving cathode front within the zirconia (and the potential implications). Finally, (5) the plasma reduction of zirconia is compared with traditional electro-chemical reduction methods.

4.1. The role of pre-existing oxygen vacancies

Yttria-stabilised zirconia (YSZ) is known to contain oxygen vacancies ($V_O^{\bullet\bullet}$) within the material as illustrated in Fig. 14a, which must form in
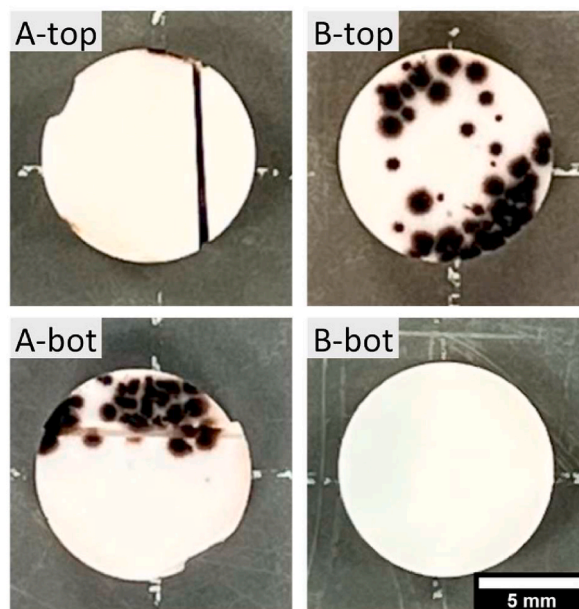
Fig. 12. Optical images of the top and bottom surfaces of zirconia samples plasma treated at 200 °C for 30 min with the cathode in contact beneath the sample (A) and above the sample (B).

response to the charge disparity between Zr^{4+} and Y^{3+} (as depicted by equation (1)) [37–40]. This development of oxygen vacancies (with no trapped electrons) acts to preserve charge neutrality across the entire material. However, despite the net neutral charge from a macroscopic scale, the presence of oxygen vacancies with less than two trapped electrons (i.e., $V_O^{\bullet\bullet}$ and $V_O^{\bullet}$) do still create localised charge disparity across the anionic sites (as these vacancies are positively charged in relation to anionic sites occupied by O^{2-} ions) [40–42].

Therefore, in the presence of a cathodic and/or anodic potential (as found during plasma treatments), this local charge disparity can be expected to lead to the segregation of charges according to their relative potential (i.e., $V_O^{\bullet\bullet}$ moving towards the cathodic side and O^{2-} sites moving towards the anodic side). If the cathodic and anodic potentials are homogeneously spread across the opposite faces of the material (as would be the case under ideal contact conditions), a uniform gradient of oxygen vacancies would be expected to be developed at each depth between the two electrodes (Fig. 14b). As the movement of oxygen vacancies can only be possible through the displacement of lattice oxygen
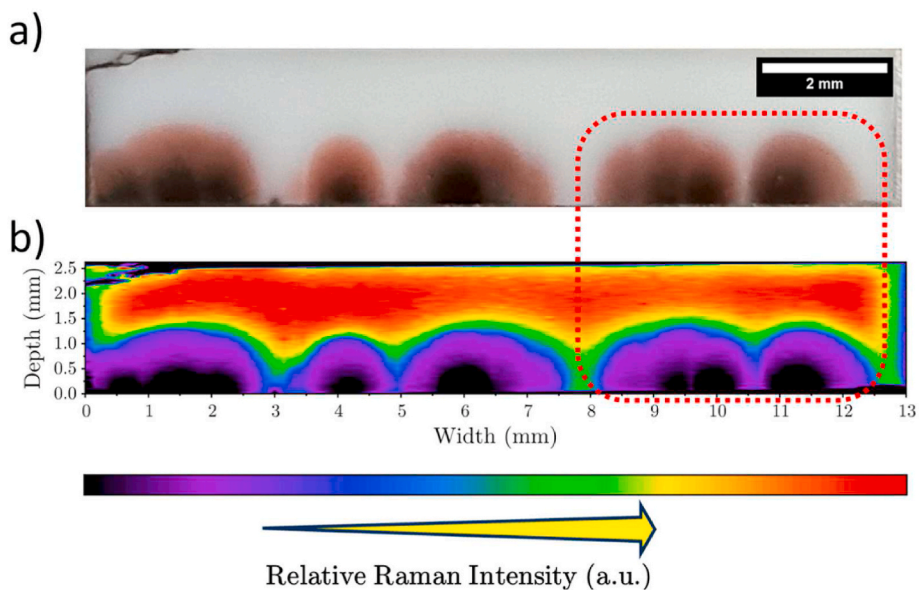
Fig. 13. Cross-sectional (a) optical image and (b) Raman intensity map of a zirconia sample plasma treated at 200 °C for 5 hours. Red dashed box corresponds to the asymmetrical growth described in 3.4.
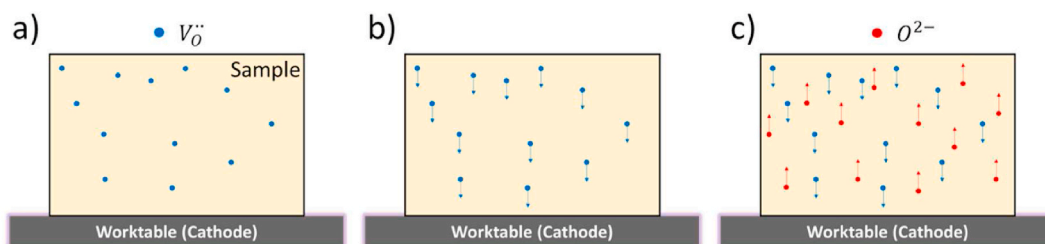
Fig. 14. Schematic diagram showing a transverse view of a zirconia sample on a cathode worktable with (a) the pre-existing oxygen vacancies, (b) the initial movement of pre-existing oxygen vacancies and (c) the opposite migration of lattice oxygen.
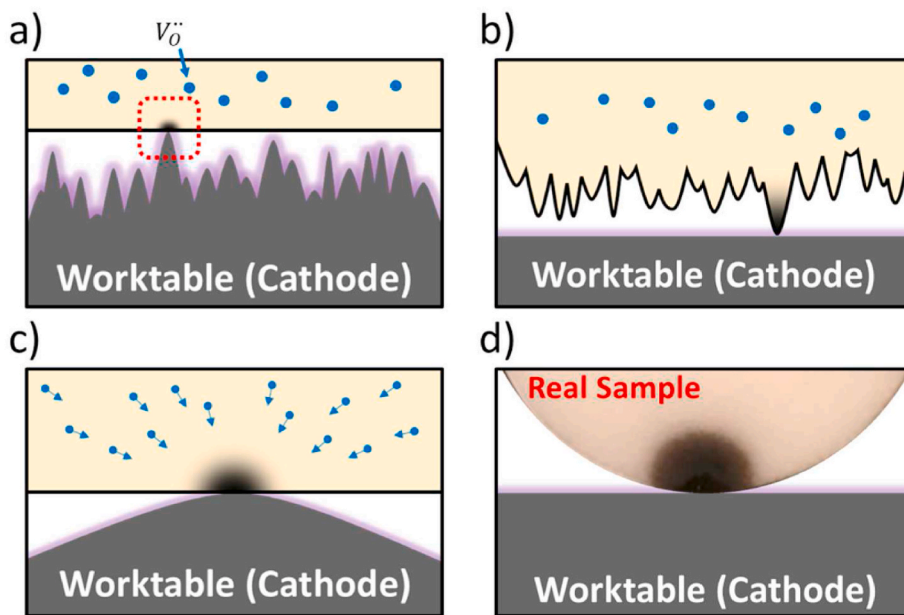
Fig. 15. Diagram showing a transverse view of a zirconia specimen with pre-existing oxygen vacancies ($V_O^{\bullet\bullet}$) under different contact conditions due to a rough worktable surface (a) or rough sample surface (b). A magnified view of a single asperity (red dashed box) with the collective directional movement of oxygen vacancies towards the contact point (c). A camera image of a cylindrical zirconia sample treated using a single contact point under DCP plasma treatment conditions at 200 °C for 5 hours (d).

atoms, an equivalent amount of lattice oxygen is considered to move in the opposite direction (i.e., from the cathode towards the anode) as illustrated in Fig. 14c. As shown by equation (2), this represents a net movement (from anode-facing sites) of oxygen vacancies towards the cathode-facing surface [$V_O^{\bullet\bullet}$(af) $\rightarrow V_O^{\bullet\bullet}$(cf)] with a net movement of lattice oxygen (from cathode-facing sites) towards the anode-facing surfaces [O_O^X (cf) $\rightarrow O_O^X$ (af)].

$$Y_2O_3 \rightarrow 2Y_{Zr}' + 3O_O^X + V_O^{\bullet\bullet} \qquad (1)$$

$$V_O^{\bullet\bullet}(\text{af}) + O_O^X (\text{cf}) \rightarrow V_O^{\bullet\bullet}(\text{cf}) + O_O^X(\text{af}) \qquad (2)$$
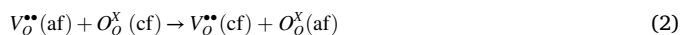
4.2. The need for cathode contact and electrical discharge

Instead of the homogeneous reduction of the zirconia following plasma treatment (as described in §4.1), localised circular black spots are observed on the surface of the samples (Figs. 7 and 8). Given that ideal flat contact between two plane surfaces (i.e., sample and worktable) is known to be extremely challenging, this suggests that ideal contact conditions are not present during these treatments. Therefore, it is more probable that the true physical contacting points between the surfaces are localised to the most protruding asperities of the two surfaces (Fig. 15a and b). This suggests that the diffusion of the oxygen vacancies towards the cathode is not uniform and is instead biased towards the sites with the strongest cathodic potential (i.e., most intimate contacting points). Confirmation of this directional migration was revealed by developing a treatment with only a single contact point with the cathodic worktable (Fig. 15c and d). Under these settings, plasma blackening was observed to only develop from a single contact point (and grew uniformly in all directions away from the contact point).

The contact dependence of the process is further supported by the findings of the treatments utilising worktables with blind holes (Fig. 10). No circular black spots could be found at sites where contact between the cathode and zirconia sample was intentionally prevented (red dashed box in Fig. 11).

The influence of voltage is well described by Paschen's law, where the breakdown voltage of a gas (or gas mixture) is a function of the pressure and distance between the electrodes [43,44]. Given that zirconia is typically non-conductive, it can be regarded as being at a floating potential that is relatively anodic to the worktable (to oppose the nearby electric field). Therefore, at close distances (or appropriate power/pressure settings), it is possible for the electric current to discharge from the cathode towards the zirconia. In practice, the discharge of current will closely relate to the gap between the asperities of the zirconia and the cathodic worktable, with greater breakdown voltage requirements for larger gaps. At sufficiently low potentials, this would give rise to only the most intimate contacting asperities being actively involved in the discharge process. Therefore, this localises the positions where significant current transfer can take place, and consequently influences the electric field distribution around the sample, and leads to non-uniform net movement of oxygen vacancies (and cation reduction) across the cathode-facing surface.

The combined findings of the blind hole (§3.3.2) and cathodic potential (§3.2.2) experiments demonstrate the critical influence that
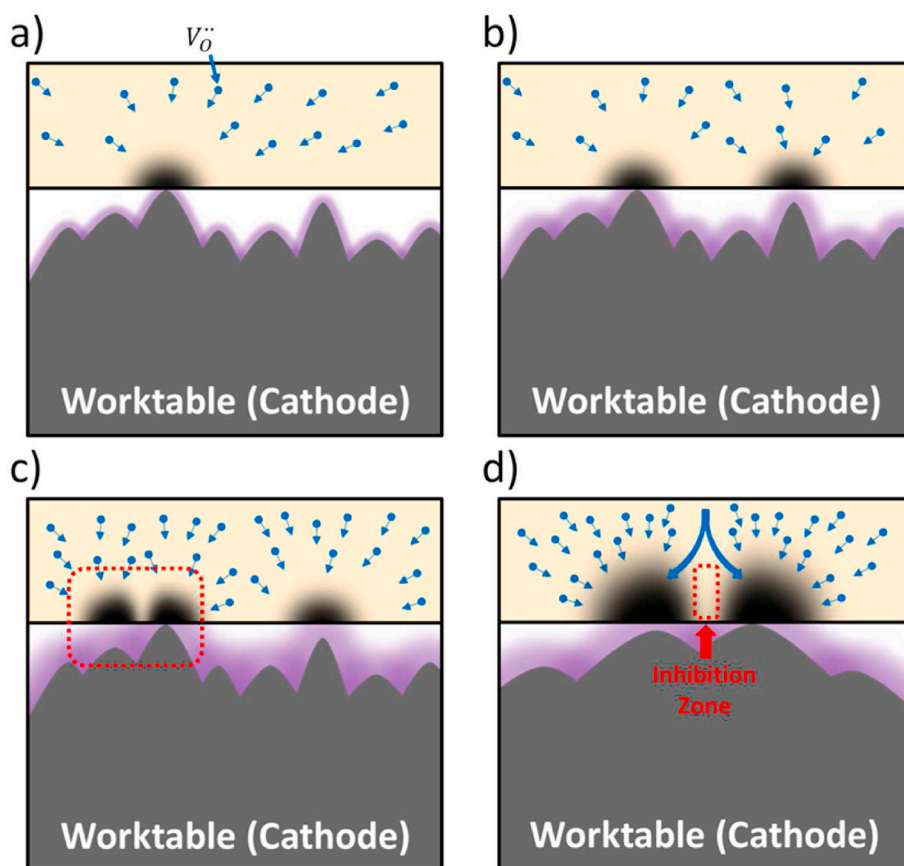
Fig. 16. Overview of the localised 'activation' of the cathode-facing surface, directed net movement of oxygen vacancies ($V_O^{\bullet\bullet}$) and the influence of nearby black regions during the initial stages of plasma treatment of zirconia. Images a) $\rightarrow$ c) show the effect of increasing cathodic potential and demonstrate the electrical breakdown of larger gaps and therefore the 'activation' of more sites on the zirconia surface. When 'active' sites are well separated (a & b), the black regions are found to grow with a hemispherical shape. However, when 'active' sites are close together (c) black regions with asymmetrical shape develop. Image d) shows a magnified view of two nearby 'active' regions (red dashed box in image c). The diversion of the net movement of oxygen vacancies between the two 'active' regions is revealed (in image d) and demonstrates how an inhibition zone (red dashed box in image d) between them can form.

contact conditions and electrical potential have on the initiation mechanism and localised bulk-reduction of zirconia. The importance of the 'active' black spots at the cathode-facing surface is also clearly demonstrated by the lack of transformation of the zirconia under ASP treatment conditions (Fig. 6), where no direct contact with the cathode is made despite interactions with other reactive species within the plasma.

Fig. 16 provides an overview of the relationship between the local cathode-to-sample spacing and applied potential, as well as their influence on the net movement of oxygen vacancies. Larger cathodic potentials are shown to allow for the breakdown of bigger gaps between the asperities of the cathode worktable and zirconia surface. This allows for the 'activation' of non-contacting asperities (indirect contact) and allows for the development of more 'active' sites (Fig. 16b). The influences of nearby 'active' sites on each other are also illustrate in Fig. 16c and will be discussed in further detail in §4.4.

4.3. Generation and conduction of new oxygen vacancies

Although oxygen vacancies exist within pristine yttria-stabilised zirconia, the total numbers are finite and cannot account for continuous collection of vacancies at the cathode-facing 'active' regions. However, as progressive transformation of zirconia is observed with longer and/or more powerful plasma treatment conditions, it must be implied that new oxygen vacancies are generated during the treatment process. The hemispherical outward growth of the black regions also supports the formation of new oxygen vacancies (from the anode-facing surfaces), which can enable continuous homogeneous net movement of oxygen vacancies from all directions. Therefore, this suggests that the environment around the anode-facing surfaces may also play a crucial role for the extensive treatment of zirconia.

The bombardment of electrically conductive workpieces with ionised gases forms the foundation of many direct current (DC) plasma treatment technologies. However, as untreated zirconia is not a good electrical conductor, no such direct bombardment would be expected to happen. Additionally, as the zirconia is not in direct contact with the anode, as is the case in electrochemical reduction methods, the driving forces for the removal of oxygen are difficult to explain. Therefore, alternative means of forming oxygen vacancies must exist. One potential way is the interaction of the exposed anode-facing surfaces with post-plasma species present within the chamber. Given that species within the plasma are highly energetic (i.e., at high temperatures), even when the collective plasma can be considered 'cold' or 'weak', it is possible for these species to overcome the Zr–O dissociation energy and thus allow for the formation of oxygen vacancies (equation (3)).

Once the oxygen vacancies are formed, their relative positive charge drives their accumulation at the 'active' sites of the cathode-facing (cf) surface (as described in §4.1). The combination of the net movement of oxygen vacancies away from the anode-facing surfaces and their replacement with lattice oxygen (equation (2) and Fig. 17) allows for the continuous generation of new oxygen vacancies throughout the plasma treatment. The cathodic potential of the worktable can then attract the (relatively) positively charged oxygen vacancies towards the 'active' sites, as well as supply the electrons necessary for the reduction of zirconium ions (Zr^{4+} to Zr^{3+}). However, the order of these processes are still unclear and requires further investigation. Moreover, the role that the electrons formed during the generation of oxygen vacancies (equation (3)) play are also unclear. It is possible for the electrons to be released away from the sample (and move towards the chamber anode) or for them to facilitate the reduction of zirconium ions at the anode-facing surfaces (as shown by equation (4)) [28,45–47].

Overall, this proposed mechanism of oxygen vacancies generation is supported by the observed effects that treatment temperature, cathodic voltage and treatment duration have on transformation of zirconia.
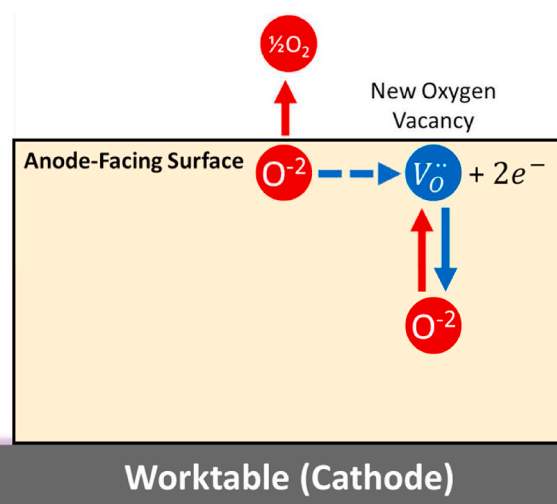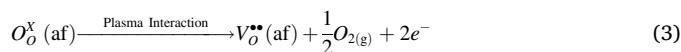

Fig. 17. Overview of the continuous removal of lattice oxygen (O^{2-}) at the anode-facing surfaces during plasma treatment of zirconia. This is made possible by the replacement of newly formed oxygen vacancies (V_O^X) with lattice oxygen coming from cathode-facing sites.

$$O_O^X \ (\text{af}) \xrightarrow{\text{Plasma Interaction}} V_O^{\bullet\bullet} (\text{af}) + \frac{1}{2}O_{2(g)} + 2e^- \tag{3}$$

$$Zr^{4+} + e^- \rightarrow Zr^{3+} \tag{4}$$

4.3.1. Influence of treatment parameters on formation and net movement of oxygen vacancies

Treatment temperature is known to directly influence the energy requirements for the dissociation of Zr–O bonds (by way of increased bond thermal energy) [48–50]. Therefore, higher temperatures can facilitate the rightward shift of equation (3), which, at the earlier stages of treatment, can be perceived as a shorter "initiation" phase (where limited or no colour change is observed). As the temperature rises, greater numbers of oxygen vacancies are generated, which increase the concentration of charge carriers, and thus increase the electrical conductivity of zirconia. The increased thermal (vibrational) energy within the zirconia crystal structure at elevated treatment temperatures also provides favourable thermodynamic and kinetic conditions necessary for diffusion (conduction) of oxygen vacancies (rightward shift of equation (2)). This can accelerate the accumulation of oxygen vacancies at the cathode-facing surface, which can be interpreted as the "migration" phase. Hence, temperature strongly correlates with the rate of transformation under plasma treatment, as evidenced by the progressive bulk transformations shown in Fig. 7.

Additionally, as greater power input (i.e., stronger plasma) is also required to achieve higher temperatures, the influence of plasma power must also be considered. As previously described in §4.2, the cathode potential can directly influence the number of 'active' sites that form on the cathode-facing surface. Therefore, it is already expected that increasing the operating voltage will directly influence the distribution and rate of bulk-reduction. Additionally, more energetic (and frequent) post-plasma species formation with stronger plasma will also aid in generating more oxygen vacancies. Finally, larger potential differences between the cathode, sample (floating potential) and anode walls of the chamber will also have an accelerating effect on the diffusion of oxygen vacancies towards the cathode. Overall, the effect of greater potential differences is to promote faster and more effective bulk-transformation of zirconia samples (as evidenced in Fig. 8).

In contrast to temperature and operating voltage, treatment duration only appears to influence the net migration and accumulation of oxygen vacancies at the cathode-facing surface. Treatment duration is found to

have no appreciable influence on initiating the transformation of the zirconia, as evidenced by the lack of change observed when insufficient temperature (or power) conditions are employed (Figs. 7 and 8). Similarly, cationic doping is also not observed to be (at least not significantly) involved in the formation and movement of oxygen vacancies during plasma treatment of zirconia (Fig. 9).

4.4. Movement and growth of cathode front

At the start of the plasma treatment of zirconia, the current transfer (both direct and indirect) takes place at the physical interface between the cathode and the cathode-facing surface of the zirconia sample (as shown in Fig. 16). However, analogous to electrochemical reduction techniques, this cathode front is found to move with the growth of the black oxygen-deficient zirconia ($ZrO_{2-\alpha}$) that initiates from the 'active' points on the cathode-facing surface.

This moving cathode front develops from the progressive migration of oxygen vacancies from all directions towards these 'active' sites, which form a concentration gradient of oxygen vacancies (and Zr^{3+} cations). This leads to growing black regions that are progressively more oxygen-deficient over time (where α continuously becomes larger). The centre of the region exhibits the best light absorption and darkest colour (i.e., where α is largest), and the areas away from this centre gradually become lighter (i.e., where α becomes smaller). This gradient of oxygen-deficiency is strongly supported by the observations (Fig. 13) of varying colour intensity (visually) and light absorption capability (under Raman mapping) of growing black regions.

As it is well established, the electrical conductivity of sub-stoichiometric zirconia ($ZrO_{2-\alpha}$) is significantly greater than stoichiometric zirconia (ZrO_2) [51–53]. As shown by equation (5), the overall formation of substoichiometric zirconia follows from the removal of (molar equivalent amount of) lattice oxygen anions.

$$ZrO_2 \rightarrow ZrO_{2-\alpha} + \frac{\alpha}{2}O_{2(g;\ mol)} \qquad (5)$$

This formation of oxygen-deficient zirconia also reduces zirconium cations ($Zr^{4+} \rightarrow Zr^{3+}$) and therefore gives rise to the occupation of new defect or mid-gap energy states (occupation of Zr 4d level) between the top of the valence band (highest occupied energy level) and the bottom of the conduction band (lowest unoccupied energy level). Consequently, the electronic bandgap of oxygen-deficient zirconia is significantly reduced as compared with the pristine structure.

This lowers the energy requirement for the valence-to-conduction band transition of electrons, which significantly enhances the light absorption capability (bandgap within the visible light range) and improves the electrical conductivity of zirconia [3,6,52,54].

Additionally, as this accumulation initiates and grows outward from the 'active' sites of the cathode-facing surface, this allows for the continuous occupation of the conduction band energy levels within these regions. The effect of this electron occupation is the propagation of the electrical current from the cathode interface to the reduced regions of the zirconia (black regions).

Effectively, this acts to extend the cathode front into the zirconia material, and as new oxygen vacancies are continuously generated and conducted towards the reduced regions, the transformed regions grow outward and become more conductive. Essentially, this forms a moving cathode front that is analogous to the moving reaction front in electrochemical reduction techniques [36].

The hemispherically growing black regions form a dynamic cathode front which increases the effective surface area of zirconia in contact with the cathode. Consequently, this mechanism regulates the lateral surface growth of the black regions at a rate consistent with that of the internal boundaries (as found within Fig. 11).

The observations of the growth trends of the black reduced regions provides strong supporting evidence for the moving cathode theory. During the early stage of growth, the black regions are typically small

enough and spread out enough to not influence each other, giving rise to hemispherical growth within the material (Fig. 16a). Hemispherical growth proceeds while the different black regions are separated (Fig. 16b); however, as the black regions approach one another, the supply of oxygen vacancies for each growing black region becomes divided. This significantly limits the growth rate of the regions between the adjacent moving fronts and results in the formation of columnar morphology between the regions (as shown by Fig. 16d). When there are many adjacent black regions, columnar shaped growth patterns are seen throughout the bulk (as shown in Fig. 7c1).

When the moving reaction front reaches the anode-facing surfaces of the sample, a direct circuit can form between the cathode, sample, and anode (going through the conductive gas atmosphere). This accelerates the transformation rate at the through-depth treated regions by enabling direct ionic bombardment of the exposed spots (as shown in Fig. 18). The formation of the plasma at the surface brings both greater quantities and more energetic impact events, thereby increasing the rate of removal of lattice oxygen and supply of fresh oxygen vacancies at the surface (equation (3)). The development of this direct bombardment has already been shown by the authors in a previous study (Fig. 1 of Ref. [28])

4.5. Comparisons between plasma reduction and electrochemical reduction

From the first reports of electrical blackening of zirconia in 1970 [42], investigations on the blackening phenomena have attracted substantial interest [13,55–66]. As investigations into the electrochemical, optical, and thermal modifications of black zirconia have advanced, numerous studies have successfully demonstrated the brightening and darkening transformation of zirconia during flash sintering. Given the similarities between flash sintering and plasma blackening (as previously described in Ref. [28]), it is valuable to compare the mechanisms and principals involved across both technologies [33,34,36].

The primary distinction between plasma treatment and traditional electro-reduction methods lies in the setup and operational principles. Under plasma treatment, the sample does not come into direct contact with the anode of the circuit. Instead, ionised gases play a crucial role in the process by providing a conductive medium for the transfer of current between the anode and cathode (i.e., completing the circuit) [67–70]. This significantly accelerates the subsequent reduction process through two ways: (1) greater effective surface area in (indirect) contact with the anode for the formation of oxygen vacancies (leading to spherical
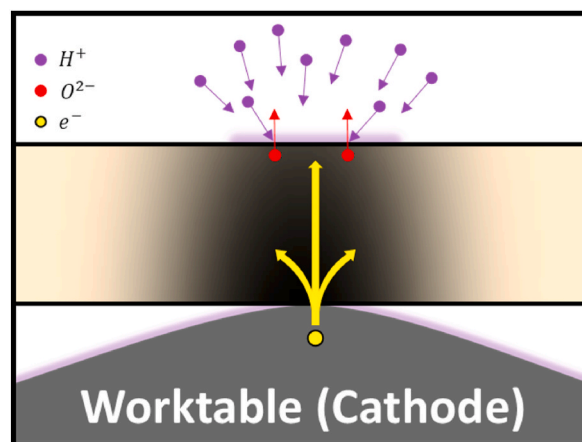

Fig. 18. Schematic representation of the formation of a glow-discharge at an anode-facing surface of zirconia following the through-depth growth of a black region. The subsequent direct bombardment with ionic species (H^+ in this case) can accelerate the removal of lattice oxygen and the formation of oxygen vacancies during the plasma treatment.

growth) and (2) strong direct plasma bombardment once the transformed regions expand to the outer surface (as shown by the accelerated bombardment with H^+ ions in Fig. 18).

As the bottom of the sample is in contact with the cathode, it is subjected to the strongest cathodic potential, while all other surfaces of the zirconia sample can be regarded as being relatively anodic in comparison. This arrangement allows oxygen to escape from various angles, as evidenced by the observed hemispherical shape and growth of the black regions in Figs. 10 and 13.

Unlike plasma treatments, electrochemical reduction typically gives rise to parallel field lines between the electrodes [71]. This typically then generates a unidirectional potential gradient and produces a unidirectional flow of current between the anode and cathode (through the sample) [36]. Therefore, this constrains the direction in which oxygen can escape, and new vacancies can be supplied for the continuous reduction, which leads to the formation of distinct finger-like growth of black regions [36].

Based on the principles of electrochemistry, the entire zirconia samples can be understood as a collection of resistors connected in parallel in the direction of the current. Consequently, the central regions (core) of the cathode-touching zirconia surfaces in electrochemical reduction approaches are more likely to overcome the breakdown voltage (as discussed in §4.2), leading to preferential reduction around those regions. However, no such phenomena is observed for plasma treated zirconia samples, with the depth of the black regions being found to be consistent between the edges and centres of the samples (Fig. 7b2 and Fig. 10). Therefore, low-pressure plasma treatment presents as a flexible and spatially unrestricted technique for the reduction of zirconia.

5. Conclusions

Bulk oxygen-deficient zirconia was successfully produced within this study using a variety of low-pressure plasma treatment configurations and parameters. Evaluation of the impact of different treatment parameters on the reduction (blackening) of zirconia has enabled the proposal of a potential mechanism for the initiation and growth of the transformed regions. Four key development stages of the transformation process are identified, namely: bulk oxygen vacancy conductance, surface activation, oxygen vacancy generation and a moving cathode front. The findings of this study are summarised as follows:

- **Bulk oxygen vacancy conductance**: The reduction (blackening) of zirconia arises due to the opposing net migrations of lattice oxygen (O^{2-}) and oxygen vacancies ($V_O^{\bullet\bullet}$) towards the anode-facing and cathode-facing surfaces, respectively.
- **Surface activation**: Transformation of zirconia is found to initiate at isolated 'active' sites that correspond to locations where there is direct contact (physically touching) or indirect contact (through the electrical breakdown of the gap) with the cathodic worktable.
- Newly formed black regions grow from the cathode-facing sites towards the anode-facing surfaces. When the 'active' sites are spread out, they grow in all directions and form hemispherical black regions.
- The change in colour of the treated material relates to the formation of oxygen-deficient zirconia ($ZrO_{2-\alpha}$). The strongest concentration of $V_O^{\bullet\bullet}$ (where α is largest) are found at the centre of the black regions (at the initiation site). When moving away from the centre, there is a gradual transition back to the white colour of the pristine material (corresponding to smaller α values).
- When the initial 'active' sites are located close together, migration of lattice oxygen and $V_O^{\bullet\bullet}$ becomes divided between the growing interfaces of both regions, leading to the formation of inhibition zones and asymmetric growth. This is found to initially produce striated columnar regions of black and white zirconia in through-depth

treated samples, which disappear with longer and/or more powerful treatments.
- **Oxygen vacancy generation**: New $V_O^{\bullet\bullet}$ are generated by the release of lattice oxygen at the anode-facing surfaces. The opposing migration of $V_O^{\bullet\bullet}$ and lattice oxygen enable continuous generation of $V_O^{\bullet\bullet}$ throughout the treatment process.
- **Moving cathode front**: The cathode reaction front, which starts at the worktable surface, expands to the growing boundaries of the black regions throughout the treatment. This increases the effective surface area of the cathode in contact with the zirconia, and forms a moving cathode front, thereby accelerating the treatment process. Oxygen vacancies, which have a positive charge relative to lattice oxygen, migrate towards this moving cathode front.
- Once the moving cathode front reach the anode-facing surface, direct ionic bombardment of the surface ensues. This significantly enhances the rate of lattice oxygen removal and oxygen vacancies formation.

In conclusion, low-pressure plasma has been demonstrated to be an attractive and scalable alternative approach for the effective bulk-reduction of zirconia. The process is shown to be adaptable and highly controllable through the optimisation of treatment configurations and parameters. It is hoped that the promising findings of this study can inspire further studies on the plasma reduction of zirconia.

Declaration of competing interest

The authors declare that they have no known competing financial interests or personal relationships that could have appeared to influence the work reported in this paper.

Acknowledgements

References

[1] Sinhamahapatra A, Jeon J-P, Kang J, Han B, Yu J-S. Oxygen-deficient zirconia (ZrO2−x): a new material for solar light absorption. Sci Rep 2016;6(1):1–8.
[2] Qi F, Yang Z, Zhang J, Wang Y, Qiu Q, Li H. Interfacial reaction-induced defect engineering: enhanced visible and near-infrared absorption of wide band gap metal oxides with abundant oxygen vacancies. ACS Appl Mater Interfaces 2020;12(49): 55417–25.
[3] Imparato C, Fantauzzi M, Passiu C, Rea I, Ricca C, Aschauer U, Sannino F, D'Errico G, De Stefano L, Rossi A. Unraveling the charge state of oxygen vacancies in ZrO2–x on the basis of synergistic computational and experimental evidence. J Phys Chem C 2019;123(18):11581–90.
[4] Jiao X, Sun L, Zhang W, Ren J, Zhang L, Cao Y, Xu Z, Kang Y, Xue P. Engineering oxygen-deficient ZrO2-x nanoplatform as therapy-activated "immunogenic cell death (ICD)" inducer to synergize photothermal-augmented sonodynamic tumor elimination in NIR-II biological window. Biomaterials 2021;272:120787.
[5] Sun L, Jiao X, Liu W, Wang Y, Cao Y, Bao S-J, Xu Z, Kang Y, Xue P. Novel oxygen-deficient zirconia (ZrO2–x) for Fluorescence/Photoacoustic Imaging-Guided photothermal/Photodynamic therapy for cancer. ACS Appl Mater Interfaces 2019; 11(44):41127–39.
[6] Wang Q, Edalati K, Koganemaru Y, Nakamura S, Watanabe M, Ishihara T, Horita Z. Photocatalytic hydrogen generation on low-bandgap black zirconia (ZrO 2) produced by high-pressure torsion. J Mater Chem A 2020;8(7):3643–50.
[7] Römer H, Luther KD, Assmus W. Coloured zirconia. Cryst Res Technol 1994;29(6): 787–94.
[8] Zhang H, Li Z, Kim B-N, Morita K, Yoshida H, Hiraga K, Sakka Y. Effect of alumina dopant on transparency of tetragonal zirconia. J Nanomater 2012;2012. 1-1.
[9] Buchanan R, Pope S. Optical and electrical properties of yttria stabilized zirconia (YSZ) crystals. J Electrochem Soc 1983;130(4):962.
[10] Vemury S, Pratsinis SE. Dopants in flame synthesis of titania. J Am Ceram Soc 1995;78(11):2984–92.
[11] Etacheri V, Seery MK, Hinder SJ, Pillai SC. Oxygen rich titania: a dopant free, high temperature stable, and visible-light active anatase photocatalyst. Adv Funct Mater 2011;21(19):3744–52.
[12] Stojadinović S, Vasilić R, Radić N, Grbić B. Zirconia films formed by plasma electrolytic oxidation: photoluminescent and photocatalytic properties. Opt Mater 2015;40:20–5.

[13] Moya JS, Moreno R, Requena J, Soria J. Black color in partially stabilized zirconia. J Am Ceram Soc 1988;71(11):C479–80.

[14] Sasaki K, Maier J. Re-analysis of defect equilibria and transport parameters in Y2O3-stabilized ZrO2 using EPR and optical relaxation. Solid State Ionics 2000;134 (3–4):303–21.

[15] Guo F, Xiao P. Effect of Fe2O3 doping on sintering of yttria-stabilized zirconia. J Eur Ceram Soc 2012;32(16):4157–64.

[16] Kumar S, Ojha AK. Oxygen vacancy induced photoluminescence properties and enhanced photocatalytic activity of ferromagnetic ZrO2 nanostructures on methylene blue dye under ultra-violet radiation. J Alloys Compd 2015;644: 654–62.

[17] Zhang J, Gao Y, Jia X, Wang J, Chen Z, Xu Y. Oxygen vacancy-rich mesoporous ZrO2 with remarkably enhanced visible-light photocatalytic performance. Sol Energy Mater Sol Cell 2018;182:113–20.

[18] Teeparthi SR, Awin EW, Kumar R. Dominating role of crystal structure over defect chemistry in black and white zirconia on visible light photocatalytic activity. Sci Rep 2018;8(1):5541.

[19] Renuka L, Anantharaju K, Sharma S, Nagabhushana H, Vidya Y, Nagaswarupa H, Prashantha S. A comparative study on the structural, optical, electrochemical and photocatalytic properties of ZrO2 nanooxide synthesized by different routes. J Alloys Compd 2017;695:382–95.

[20] Reddy CV, Reddy IN, Ravindranadh K, Reddy KR, Kim D, Shim J. Ni-dopant concentration effect of ZrO2 photocatalyst on photoelectrochemical water splitting and efficient removal of toxic organic pollutants. Separ Purif Technol 2020;252: 117352.

[21] Reddy CV, Babu B, Reddy IN, Shim J. Synthesis and characterization of pure tetragonal ZrO2 nanoparticles with enhanced photocatalytic activity. Ceram Int 2018;44(6):6940–8.

[22] Liu Y, Ishihara A, Mitsushima S, Ota K-i. Influence of sputtering power on oxygen reduction reaction activity of zirconium oxides prepared by radio frequency reactive sputtering. Electrochim Acta 2010;55(3):1239–44.

[23] Zu D, Wang H, Yang T, Wei H, Sun S, Wu H. Black ZrO2 synthesized by molten lithium reduction strategy for photocatalytic hydrogen generation. J Am Ceram Soc 2020;103(8):4035–42.

[24] Choi E-Y, Heo DH. Reduction of zirconium oxide compounds by lithium metal as a reductant in molten LiCl salt. J Nucl Mater 2018;512:193–8.

[25] Azarian MH, Mahmood WAK. In-situ sol–gel synthesis of zirconia networks in flexible and conductive composite films. J Appl Polym Sci 2020;137(46):49506.

[26] Suleiman RK, Kumar AM, Rahman MM, Al-Badour FA, Meliani MH, Saleh TA. Effect of metal oxide additives on the structural and barrier properties of a hybrid organosilicon sol-gel coating in 3.5% NaCl medium. Prog Org Coating 2020;148: 105825.

[27] Qi F, Yang Z, Wang Y, Qiu Q, Li H. Defects in black zirconia responsible for solar energy harvesting. J Mater Chem C 2021;9(46):16732–40.

[28] Dashtbozorg B, Shi F, Tagliaferro A, Abela S, Falticeanu L, Dong H. Plasma defect-engineering of bulk oxygen-deficient zirconia. Acta Mater 2023:119457.

[29] Dashtbozorg B, Tao X, Dong H. Active-screen plasma surface multi-functionalisation of biopolymers and carbon-based materials–an overview. Surf Coating Technol 2022;442:128188.

[30] Nakajima H, Itoh K, Kaneko H, Tamaura Y. Effects of Fe doping on crystalline and optical properties of yttria-stabilized zirconia. J Phys Chem Solid 2007;68(10): 1946–50.

[31] Lv H, Bao J, Ruan F, Zhou F, Wang Q, Zhang W, Guo W, Zhang Y, Song X, An S. Preparation and properties of black Ti-doped zirconia ceramics. J Mater Res Technol 2020;9(3):6201–8.

[32] Nakajima H, Ishihara K, Shen Q, Toyoda T, Itoh K, Kaneko H, Tamaura Y. Effect of Fe doping on photoluminescence of yttria-stabilized zirconia. J Alloys Compd 2007;441(1–2):255–8.

[33] Alvarez A, Dong Y, Chen IW. DC electrical degradation of YSZ: voltage-controlled electrical metallization of a fast ion conducting insulator. J Am Ceram Soc 2020; 103(5):3178–93.

[34] Biesuz M, Pinter L, Saunders T, Reece M, Binner J, Sglavo VM, Grasso S. Investigation of electrochemical, optical and thermal effects during flash sintering of 8YSZ. Materials 2018;11(7):1214.

[35] Christian KH, Charalambous H, Jha SK, Tsakalakos T. Current-ramp assisted sintering of 3YSZ: electrochemical and microstructural comparison to flash and thermal sintering. J Eur Ceram Soc 2020;40(2):436–43.

[36] Janek J, Korte C. Electrochemical blackening of yttria-stabilized zirconia–morphological instability of the moving reaction front. Solid State Ionics 1999;116(3–4):181–95.

[37] Chen X, Khor K, Chan S, Yu L. Influence of microstructure on the ionic conductivity of yttria-stabilized zirconia electrolyte. Mater Sci Eng, A 2002;335(1–2):246–52.

[38] Masó N, West AR. Electronic conductivity in yttria-stabilized zirconia under a small dc bias. Chem Mater 2015;27(5):1552–8.

[39] Han P, Worrell W. Mixed (oxygen ion and p-Type) conductivity in yttria-stabilized zirconia containing Terbia. J Electrochem Soc 1995;142(12):4235.

[40] Dong Y, Huang Y, Ding D, Wu W, Yao X, Li J. Chemical and structural origin of hole states in yttria-stabilized zirconia. Acta Mater 2021;203:116487.

[41] Zhang L, Zhu L, Virkar AV. Electronic conductivity measurement of yttria-stabilized zirconia solid electrolytes by a transient technique. J Power Sources 2016;302:98–106.

[42] Casselton R. Low field DC conduction in yttria-stabilized zirconia. Phys Status Solidi 1970;2(3):571–85.

[43] Paschen law for argon glow discharge. In: Torres C, Reyes P, Castillo F, Martínez H, editors. Journal of Physics: Conference series. IOP Publishing; 2012.

[44] Loveless AM, Garner AL. A universal theory for gas breakdown from microscale to the classical Paschen law. Phys Plasmas 2017;24(11).

[45] Morinaga M, Adachi H, Tsukada M. Electronic structure and phase stability of ZrO2. J Phys Chem Solid 1983;44(4):301–6.

[46] Liu Q-J, Liu Z-T, Feng L-P. Elasticity, electronic structure, chemical bonding and optical properties of monoclinic ZrO2 from first-principles. Phys B Condens Matter 2011;406(3):345–50.

[47] Králik B, Chang EK, Louie SG. Structural properties and quasiparticle band structure of zirconia. Phys Rev B 1998;57(12):7027.

[48] Chupka W, Berkowitz J, Inghram MG. Thermodynamics of the Zr-ZrO2 system: the dissociation energies of ZrO and ZrO2. J Chem Phys 1957;26(5):1207–10.

[49] Murad E, Hildenbrand D. Thermochemical properties of gaseous ZrO and ZrO2. J Chem Phys 1975;63(3):1133–9.

[50] Murali M, Bijani C, Daran J-C, Manoury E, Poli R. Acetate exchange mechanism on a Zr 12 oxo hydroxo cluster: relevance for reshaping Zr–carboxylate coordination adaptable networks. Chem Sci 2023;14(30):8152–63.

[51] Kim YJ, Kim G-Y, Kim H-S, Kim S, Kim B, Choi YJ, Kim J, Kim J, Ryu W-H. Highly conductive ZrO2–x spheres as bifunctional framework stabilizers and gas evolution relievers in nickel-rich layered cathodes for lithium-ion batteries. Compos B Eng 2022;238:109911.

[52] Sinhamahapatra A, Jeon J-P, Kang J, Han B, Yu J-S. Oxygen-deficient zirconia (ZrO2−x): a new material for solar light absorption. Sci Rep 2016;6(1):27218.

[53] Kurapova OY, Glumov O, Pivovarov M, Golubev S, Konakov V. Structure and conductivity of calcia stabilized zirconia ceramics, manufactured from freeze-dried nanopowder. Rev Adv Mater Sci 2017;52(1–2):134–41.

[54] Din LMU, Kumar V. Oxygen-deficient low band gap black zirconia nanoparticle synthesis and tailoring its band gap/photoluminescence via silver doping. Phys B Condens Matter 2023;652:414626.

[55] Wright D, Thorp J, Aypar A, Buckley H. Optical absorption in current-blackened yttria-stabilized zirconia. J Mater Sci 1973;8:876–82.

[56] Nagle D, PaiVerneker V, Petelin A, Groff G. Optical absorption of electrolytically colored single crystals of yttria-stabilized zirconia. Mater Res Bull 1989;24(5): 619–23.

[57] PaiVerneker V, Petelin A, Crowne F, Nagle D. Color-center-induced band-gap shift in yttria-stabilized zirconia. Phys Rev B 1989;40(12):8555.

[58] Bonola C, Camagni P, Chiodelli P, Samoggia G. Study of defects introduced by electroreduction in YSZ. Radiat Eff Defect Solid 1991;119(1):457–62.

[59] Thorp J, Aypar A, Ross J. Electron spin resonance in single crystal yttria stabilized zirconia. J Mater Sci 1972;7:729–34.

[60] Shinar J, Tannhauser D, Silver B. ESR study of color centers in yttria stabilized zirconia. Solid State Commun 1985;56(2):221–3.

[61] Ben-Michael R, Tannhauser D, Genossar J. ESR centers in reduced stabilized zirconia. Phys Rev B 1991;43(10):7395.

[62] Azzoni C, Paleari A. EPR study of electron traps in x-ray-irradiated yttria-stabilized zirconia. Phys Rev B 1989;40(10):6518.

[63] Osendi MI, Moya JS, Serna CJ, Soria J. Metastability of tetragonal zirconia powders. J Am Ceram Soc 1985;68(3):135–9.

[64] Casselton RE, Penny J, Reynolds M. Structural consequences of blackening in yttria-stabilized zirconia. Newcastle upon Tyne, Eng.: International Research and Development Co. Ltd.; 1971.

[65] Moghadam F, Yamashita T, Stevenson D. Characterization of the current-blackening phenomena in scandia stabilized zirconia using transmission electron microscopy. J Mater Sci 1983;18:2255–9.

[66] Lévy M, Fouletier J, Kleitz M. Electronic conductivity of non stoichiometric yttria-doped ceria. J Phys Colloq 1980;41(C6). C6-335-C336-339.

[67] Wang J, Xiong J, Peng Q, Fan H, Wang Y, Li G, Shen B. Effects of DC plasma nitriding parameters on microstructure and properties of 304L stainless steel. Mater Char 2009;60(3):197–203.

[68] Klein A, Cardoso R, Pavanati H, Binder C, Maliska A, Hammes G, Fusao D, Seeber A, Brunatto Sy, Muzart J. DC plasma technology applied to powder metallurgy: an overview. Plasma Sci Technol 2013;15(1):70.

[69] Li C. Active screen plasma nitriding–an overview. Surf Eng 2010;26(1–2):135–41.

[70] Zhao C, Li C, Dong H, Bell T. Study on the active screen plasma nitriding and its nitriding mechanism. Surf Coating Technol 2006;201(6):2320–5.

[71] Guillon O, Elsässer C, Gutfleisch O, Janek J, Korte-Kerzel S, Raabe D, Volkert CA. Manipulation of matter by electric and magnetic fields: toward novel synthesis and processing routes of inorganic materials. Mater Today 2018;21(5):527–36.